**J. Cent. South Univ.** (2015) 22: 2825−2832
**DOI:** 10.1007/s11771-015-2814-1

Springer

# Theoretical investigation of micropolar fluid flow between two porous disks

P. Valipour[1], S. E. Ghasemi[2], M. Vatani[3]

1. Department of Textile and Apparel, Qaemshahr Branch, Islamic Azad University, Qaemshahr, Iran;
2. Young Researchers and Elite Club, Qaemshahr Branch, Islamic Azad University, Qaemshahr, Iran;
3. Department of Mechanical Engineering, Babol University of Technology, Babol, Iran



**Abstract:** The steady, laminar, incompressible and two dimensional micropolar flow between two porous disks was investigated using optimal homotopy asymptotic method (OHAM) and fourth order Runge–Kutta numerical method. Comparison between OHAM and numerical method shows that OHAM is an exact and high efficient method for solving these kinds of problems. The results are presented to study the velocity and rotation profiles for different physical parameters such as Reynolds number, vortex viscosity parameter, spin gradient viscosity and microinertia density parameter. As an important outcome, the magnitude of the microrotation increases with an increase in the values of injection velocity while it decreases by increasing the values of suction velocity.

**Key words:** theoretical investigation; porous disks; micropolar fluid flow; optimal homotopy asymptotic method (OHAM); microrotation

## 1 Introduction

The fluid flow through parallel disks has been considered due to its scientific and engineering applications such as gas turbine engines, computer storage devices, thrust bearings, radial diffusers, and biomechanics. Von KARMAN [1] firstly analyzed the steady flow of Newtonian fluid over rotating disk by using similarity transformation. ASHRAF et al [2] utilized numerical method to study the fluid flow between an impermeable disk and a permeable disk. They investigated the effects of the Reynolds number and the micropolar parameters on the velocity and rotation profiles of the flow. NAZIR and MAHMOOD [3] investigated flow and heat transfer of viscous fluid between heated contracting rotating disks. They used von KARMAN similarity transformations to reduce the Navier–Stokes equations to a system of ordinary differential equations. The analysis shows that the velocity components and especially radial component of velocity have a strong influence on the temperature distribution inside the flow regime. SI et al [4] examined the laminar flow on heat transfer of viscous fluid between two heated contracting rotating disks considering the viscous dissipation effects in the energy equation or not. IBRAHIM [5] studied the unsteady flow of a viscous incompressible fluid between two parallel disks. The governing Navier-Stokes and energy equations are transformed to a system of ordinary differential equations. The results show that the rotation of two disks has a little effect on the heat transfer process, while the rapid normal motion of the upper disk has a powerful effect on the temperature of the fluid. ERSOY [6] studied the flow of a viscous fluid between two disks rotating about distinct vertical axes at different speeds. HATAMI et al [7] investigated the asymmetric laminar flow and heat transfer of nanofluid between contracting rotating disks. HATAMI and GANJI [8] examined heat transfer and flow of nanofluid through two parallel disks in suction and blowing process in the presence of the magnetic field.

A general theory of micropolar fluid has been introduced by ERINGEN [9] in order to describe some physical systems which do not satisfy the Navier-Stokes equations. His theory includes new material parameters of the flow and new constitutive equations for Newtonian fluid flows. Later, the development of the theory is motivated by the need to model the flow of non-Newtonian fluids containing rotating micro-constituents. Many studies show that the model has a wide range of applications in blood flow, polymeric suspensions, lubricants and turbulent shear flows.

In this section, a review of the related works which principally concerns the solution of the flow and heat transfer of micropolar fluid between two parallel disks is reported. ANWAR et al [10] examined the steady, incompressible and laminar flow of a micropolar fluid

**Received date:** 2014−08−01; **Accepted date:** 2015−01−16
**Corresponding author:** S. E. Ghasemi, PhD Candidate; Tel/Fax: +98−111−3234205; E-mail: s.ebrahim.ghasemi@gmail.com

driven by injection between two porous coaxial disks. The numerical study of axisymmetry of an electrically conducting micropolar fluid between two porous disks was considered by ASHRAF and WEHGAL [11]. DARVISHI et al [12] investigated the flow of micropolar fluid in a porous channel with expanding and contracting walls. They applied spectral homotopy analysis collocation method to obtain a series solution for the flow.

Motivated by the above mentioned work, the aim of this study is to obtain the approximate solution of the micropolar flow between two porous disks. By applying an extension of von KARMAN's similarity transformations, we reduce the governing partial differential equations to a system of ordinary differential equations. Recently, several analytical methods have been applied in many engineering problems by GHASEMI et al [13−17], but to solve the governing equations of this problem, one of the newest analytical methods named optimal homotopy asymptotic method (OHAM) is used. This method is one of the strong and effective methods for solving nonlinear problems and is investigated and developed by some authors to solve nonlinear equations arising in engineering problems [18−21].

## 2 Description of problem

The steady, laminar and incompressible flow of micropolar fluid between two parallel porous disks is considered. The micropolar fluid is uniformly injected at a constant velocity $v$ through the upper disk. The flow is fully developed and the effects of the body couples and body forces are neglected.

As shown in Fig. 1, a cylindrical coordinate system may be chosen with the origin at the center between porous disks. Two stationary porous disks of radius $R_0$ are located at the plane ($z$=±$L$) and the centers of the disks coincide with the axis ($r$=0). Consider $u$ and $w$ as the velocity components in the direction of $r$- and $z$-axes, respectively. Assume that $N$ is the microrotation of the flow. Under these assumptions, the governing equations of the flow can be expressed as follows:

$$\frac{\partial u}{\partial r}+\frac{u}{r}+\frac{\partial w}{\partial z}=0 \tag{1}$$

$$(\nu+\frac{\kappa}{\rho})(\frac{\partial^2 u}{\partial r^2}+(\frac{1}{r})\frac{\partial u}{\partial r}-\frac{u}{r^2}+\frac{\partial^2 u}{\partial z^2})-\frac{\kappa}{\rho}\frac{\partial N}{\partial z}-\frac{1}{\rho}\frac{\partial p}{\partial r}=(u\frac{\partial u}{\partial r}+w\frac{\partial u}{\partial z}) \tag{2}$$

$$(\nu+\frac{\kappa}{\rho})(\frac{\partial^2 w}{\partial r^2}+(\frac{1}{r})\frac{\partial w}{\partial r}+\frac{\partial^2 w}{\partial z^2})+\frac{\kappa}{\rho}(\frac{\partial N}{\partial r}+\frac{N}{r})-\frac{1}{\rho}\frac{\partial p}{\partial z}=(u\frac{\partial w}{\partial r}+w\frac{\partial w}{\partial z}) \tag{3}$$

$$\gamma(\frac{\partial^2 N}{\partial r^2}+(\frac{1}{r})\frac{\partial N}{\partial r}-\frac{N}{r^2}+\frac{\partial^2 N}{\partial z^2})+\kappa(\frac{\partial u}{\partial z}-\frac{\partial w}{\partial r})-2\kappa N=\rho j(u\frac{\partial N}{\partial r}+w\frac{\partial N}{\partial z}) \tag{4}$$

where $\rho$ and $v$ are the density and kinematic viscosity, respectively; $j$ is the microinteria viscosity; $\kappa$ and $\gamma$ are the microrotation parameter and spin gradient viscosity, respectively.

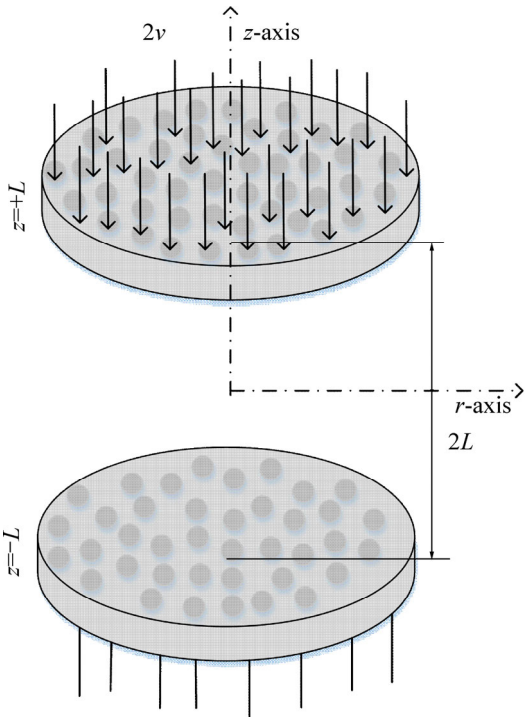


**Fig. 1** Model for micropolar fluid flow between two porous disks

The boundary condition at the two lower and upper disks for the velocity and microrotation field can be written as

$$\begin{cases}u(r,\pm L)=0\\ w(r,-L)=0,\ w(r,L)=2v\\ \phi(r,\pm L)=0\end{cases} \tag{5}$$

Notice that as the fluid is extracted from the lower disk, the velocity $v$ is assumed to be positive, and if it is injected through the upper disk, the velocity will be negative.

Define the following extension of von KARMAN's similarity transformations [1]:

$$u=-rF'(z),\quad w=2F(z),\quad \phi=-rG(z) \tag{6}$$

By substituting Eq. (6) into Eqs. (2), (3) and (4), we have

$$(\mu+\kappa)F^{(iv)}-\kappa G''-2\rho FF''=0 \tag{7}$$

where $\partial^2 p/\partial r\partial z=0$.

$$\gamma G'' + \kappa F'' - 2\kappa G - \rho j(F'G - 2FG') = 0 \quad (8)$$

Define the following parameters:

$$f(\eta) = \frac{F(z)}{v}, \quad g(\eta) = \frac{L^2 G(z)}{v}, \quad \eta = \frac{z}{L} \quad (9)$$

Upon substituting Eq. (9) into Eqs. (7) and (8) , one obtains the following equations:

$$f^{(iv)} - c_1 g'' - 2Reff''' = 0 \quad (10)$$

$$g'' + c_2(f'' - 2g) - c_3(f'g - 2fg') = 0 \quad (11)$$

where $Re = \rho VL/(\mu + \kappa)$ is the Reynlods number and $c_1 = \kappa/(\mu + \kappa)$, $c_2 = \kappa L^2/\gamma$, $c_3 = \rho jLV/\gamma$ are the vortex viscosity parameter, the spin gradient viscosity parameter and the microinertia density parameter, respectively. Here, $c_1$, $c_2$ and $c_3$ are the micropolar parameters.

The boundary condition in the dimensionless form can be written as

$$\begin{cases} f(\eta) = -1, \quad f'(\eta) = 0, \quad g(\eta) = 0, \quad \eta = -1 \\ f(\eta) = 1, \quad f'(\eta) = 0, \quad g(\eta) = 0, \quad \eta = 1 \end{cases} \quad (12)$$

## 3 Basic idea of optimal homotopy asymptotic method (OHAM)

The following nonlinear differential equation is considered:

$$\begin{cases} L(u(\tau)) + N(u(\tau)) + g(\tau) = 0 \\ \text{s.t. } B(u) = 0 \end{cases} \quad (13)$$

where $L$ is a linear operator, $N$ is a nonlinear operator, $u(\tau)$ is an unknown function, $g(\tau)$ is a known analytical function and $B$ is a boundary operator.

By means of OHAM, one first constructs a set of equations [22]:

$$(1-p)[L(\phi(\tau,p)) + g(\tau)] - H(p)[L(\phi(\tau,p)) + g(\tau) + N(\phi(\tau,p))] = 0 \quad (14)$$

And the boundary condition is

$$B(\phi(\tau,p)) = 0 \quad (15)$$

where $\phi(\tau, p)$ is an unknown function, $p \in [0, 1]$ is an embedding parameter and $H(p)$ denotes a nonzero auxiliary function for $p \neq 0$ and $H(0)=0$. So, when $p=0$ and $p=1$, it holds that

$$\phi(\tau,0) = u_0(\tau), \quad \phi(\tau,1) = u(\tau) \quad (16)$$

Thus, when $p$ increases from 0 to 1, the solution $\phi(\tau, p)$ approaches from initial solution $u_0(\tau)$ to the solution $u_0(\tau)$, where $u_0(\tau)$ is obtained from Eq. (14) when $p=0$.

$$L(u_0(\tau)) + g(\tau) = 0, \quad B(u_0) = 0$$

Consider the auxiliary function, $H(p)$, in the form:

$$H(p) = pC_1 + p^2 C_2 + \cdots \quad (17)$$

where $C_1$, $C_2$, ⋯ are constants which can be determined later.

Expand $\phi(\tau, p)$ in a series with respect to $p$ in the following manner:

$$\phi(\tau, p, C_i) = u_0(\tau) + \sum_{k \geq 1} u_k(\tau, C_i) p_k, \quad i = 1, 2, \cdots \quad (18)$$

Substituting Eq. (18) into Eq. (14), collecting the same powers of $p$, and equating the coefficient of like powers of $p$ to zero, the set of differential equation with boundary conditions is obtained. Thus, we obtain $u_0(\tau)$, $u_1(\tau, C_1)$, $u_2(\tau, C_3)$, ⋯ by solving differential equation with boundary conditions. Generally speaking, the solution of Eq. (13) can be determined approximately in the form of

$$\tilde{u}^{(m)} = u_0(t) + \sum_{k=1}^{m} u_k(\tau, C_i) \quad (19)$$

Substituting Eq. (19) in Eq. (13), it results the following expression for residual:

$$R(\tau, C_i) = L(\tilde{u}^{(m)}(\tau, C_i)) + g(\tau) + N(\tilde{u}^{(m)}(\tau, C_i)) \quad (20)$$

If $R(\tau, C_i)=0$, then $\tilde{u}(\tau, C_i)$ is the exact solution of the problem. Generally, it does not happen, especially in nonlinear problems, but we can minimize the functional:

$$J(C_1, C_2, \cdots, C_n) = \int_a^b R^2(\tau, C_1, C_2, \cdots, C_m) \mathrm{d}\tau \quad (21)$$

And the constants $C_i$ can be determined from the conditions:

$$\frac{\partial J}{\partial C_1} = \frac{\partial J}{\partial C_2} = \cdots = 0 \quad (22)$$

## 4 Application of optimal homotopy asymptotic method (OHAM)

In this section, we try to solve Eqs. (10) and (11) using OHAM. Consider $f(\eta)$, $H_1(p)$, $g(\eta)$ and $H_2(p)$ as the following:

$$\begin{cases} f(\eta) = f_0(\eta) + pf_1(\eta) + p^2 f_2(\eta) + p^3 f_3(\eta) \\ H_1(p) = pd_1 + p^2 d_2 + p^3 d_3 \\ g(\eta) = g_0(\eta) + pg_1(\eta) + p^2 g_2(\eta) + p^3 g_3(\eta) \\ H_2(p) = pe_1 + p^2 e_2 + p^3 e_3 \end{cases} \quad (23)$$

Substitute $f(\eta)$, $g(\eta)$, $H_1(p)$ and $H_2(p)$ from Eq. (23) into Eqs. (10) and (11) and rearrange them based on the powers of $p$-terms.

$p^0$:

$$\begin{cases}\dfrac{\mathrm{d}^4}{\mathrm{d}\eta^4}f_0(\eta)=0\\ \dfrac{\mathrm{d}^2}{\mathrm{d}\eta^2}g_0(\eta)=0\\ f_0(-1)=-1,\ f_0(1)=1,\ f_0'(1)=0,\ f_0'(-1)=0\\ g_0(-1)=0,\ g_0(1)=0\end{cases} \tag{24}$$

$p^1$:

$$\begin{cases} d_1\left(\dfrac{\mathrm{d}^4}{\mathrm{d}\eta^4}f_0(\eta)\right)+\dfrac{\mathrm{d}^4}{\mathrm{d}\eta^4}f_1(\eta)-\left(\dfrac{\mathrm{d}^4}{\mathrm{d}\eta^4}f_0(\eta)\right)-\\ \quad 2d_1f_0(\eta)\left(\dfrac{\mathrm{d}^3}{\mathrm{d}\eta^3}f_0(\eta)\right)-d_1\left(\dfrac{\mathrm{d}^2}{\mathrm{d}\eta^2}g_0(\eta)\right)=0\\ e_1\left(\dfrac{\mathrm{d}^2}{\mathrm{d}\eta^2}g_0(\eta)\right)+\dfrac{\mathrm{d}^2}{\mathrm{d}\eta^2}g_1(\eta)+2e_1f_0(\eta)\left(\dfrac{\mathrm{d}}{\mathrm{d}\eta}g_0(\eta)\right)-\\ \quad e_1g_0(\eta)\left(\dfrac{\mathrm{d}}{\mathrm{d}\eta}f_0(\eta)\right)-\left(\dfrac{\mathrm{d}^2}{\mathrm{d}\eta^2}g_0(\eta)\right)-\\ \quad 2e_1g_0(\eta)+e_1\left(\dfrac{\mathrm{d}^2}{\mathrm{d}\eta^2}f_0(\eta)\right)=0\\ f_1(-1)=0,\ f_1(1)=0,\ f_1'(1)=0,\ f_1'(-1)=0\\ g_1(-1)=0,\ g_1(1)=0\end{cases} \tag{25}$$

$p^2$:

$$\left(\frac{\mathrm{d}^4}{\mathrm{d}\eta^4}f_2(\eta)\right)-2d_2f_0(\eta)\left(\frac{\mathrm{d}^3}{\mathrm{d}\eta^3}f_0(\eta)\right)-2d_1f_0(\eta)\cdot\left(\frac{\mathrm{d}^3}{\mathrm{d}\eta^3}f_1(\eta)\right)+d_2\left(\frac{\mathrm{d}^4}{\mathrm{d}\eta^4}f_0(\eta)\right)-d_2\left(\frac{\mathrm{d}^2}{\mathrm{d}\eta^2}g_0(\eta)\right)-d_1\left(\frac{\mathrm{d}^2}{\mathrm{d}\eta^2}g_1(\eta)\right)+d_1\left(\frac{\mathrm{d}^4}{\mathrm{d}\eta^4}f_1(\eta)\right)-2d_1f_1(\eta)\cdot\left(\frac{\mathrm{d}^3}{\mathrm{d}\eta^3}f_0(\eta)\right)=0 \tag{26a}$$

$$\left(\frac{\mathrm{d}^2}{\mathrm{d}\eta^2}g_2(\eta)\right)-e_2g_0(\eta)\left(\frac{\mathrm{d}}{\mathrm{d}\eta}f_0(\eta)\right)-e_1g_1(\eta)\cdot\left(\frac{\mathrm{d}}{\mathrm{d}\eta}f_0(\eta)\right)+2e_2f_0(\eta)\left(\frac{\mathrm{d}}{\mathrm{d}\eta}g_0(\eta)\right)+e_1\left(\frac{\mathrm{d}^2}{\mathrm{d}\eta^2}g_1(\eta)\right)-e_1g_0(\eta)\left(\frac{\mathrm{d}}{\mathrm{d}\eta}f_1(\eta)\right)-2e_1\left(g_1(\eta)\right)+e_1\left(\frac{\mathrm{d}^2}{\mathrm{d}\eta^2}f_1(\eta)\right)+2e_1f_0(\eta)\left(\frac{\mathrm{d}^2}{\mathrm{d}\eta^2}g_1(\eta)\right)+e_2\left(\frac{\mathrm{d}^2}{\mathrm{d}\eta^2}g_0(\eta)\right)-\left(\frac{\mathrm{d}^2}{\mathrm{d}\eta^2}g_1(\eta)\right)+e_2\left(\frac{\mathrm{d}^2}{\mathrm{d}\eta^2}f_0(\eta)\right)-2e_2g_0(\eta)+2e_1f_1(\eta)\cdot\left(\frac{\mathrm{d}}{\mathrm{d}\eta}g_0(\eta)\right)=0 \tag{26b}$$

$$f_2(-1)=0,\ f_2(1)=0,\ f_2'(1)=0,\ f_2'(-1)=0 \tag{26c}$$

$$g_2(-1)=0,\ g_2(1)=0 \tag{26d}$$

$p^3$:

$$-2d_1f_0(\eta)\left(\frac{\mathrm{d}^3}{\mathrm{d}\eta^3}f_2(\eta)\right)+\left(\frac{\mathrm{d}^4}{\mathrm{d}\eta^4}f_3(\eta)\right)-d_3\left(\frac{\mathrm{d}^2}{\mathrm{d}\eta^2}g_0(\eta)\right)+d_3\left(\frac{\mathrm{d}^4}{\mathrm{d}\eta^4}f_0(\eta)\right)-\left(\frac{\mathrm{d}^4}{\mathrm{d}\eta^4}f_2(\eta)\right)-d_1\left(\frac{\mathrm{d}^2}{\mathrm{d}\eta^2}g_2(\eta)\right)-2d_3f_0(\eta)\left(\frac{\mathrm{d}^3}{\mathrm{d}\eta^3}f_0(\eta)\right)+d_2\left(\frac{\mathrm{d}^4}{\mathrm{d}\eta^4}f_1(\eta)\right)-2d_1f_1(\eta)\left(\frac{\mathrm{d}^3}{\mathrm{d}\eta^3}f_1(\eta)\right)+d_1\left(\frac{\mathrm{d}^4}{\mathrm{d}\eta^4}f_2(\eta)\right)-2d_1f_2(\eta)\left(\frac{\mathrm{d}^3}{\mathrm{d}\eta^3}f_0(\eta)\right)-2d_2f_1(\eta)\left(\frac{\mathrm{d}^3}{\mathrm{d}\eta^3}f_0(\eta)\right)-d_2\left(\frac{\mathrm{d}^2}{\mathrm{d}\eta^2}g_1(\eta)\right)-2d_2f_0(\eta)\left(\frac{\mathrm{d}^3}{\mathrm{d}\eta^3}f_1(\eta)\right)=0 \tag{27a}$$

$$e_1\left(\frac{\mathrm{d}^2}{\mathrm{d}\eta^2}g_2(\eta)\right)-e_1g_0(\eta)\left(\frac{\mathrm{d}}{\mathrm{d}\eta}f_2(\eta)\right)+2e_3f_0(\eta)\cdot\left(\frac{\mathrm{d}}{\mathrm{d}\eta}g_0(\eta)\right)-2e_3g_0(\eta)-e_2g_1(\eta)\left(\frac{\mathrm{d}}{\mathrm{d}\eta}f_0(\eta)\right)+e_1\left(\frac{\mathrm{d}^2}{\mathrm{d}\eta^2}f_2(\eta)\right)+2e_2f_1(\eta)\left(\frac{\mathrm{d}}{\mathrm{d}\eta}g_0(\eta)\right)+e_3\left(\frac{\mathrm{d}^2}{\mathrm{d}\eta^2}g_0(\eta)\right)-e_3g_0(\eta)\left(\frac{\mathrm{d}}{\mathrm{d}\eta}f_0(\eta)\right)-e_1g_1(\eta)\cdot\left(\frac{\mathrm{d}}{\mathrm{d}\eta}f_1(\eta)\right)-e_1g_2(\eta)\left(\frac{\mathrm{d}}{\mathrm{d}\eta}f_0(\eta)\right)-2e_2g_1(\eta)-\left(\frac{\mathrm{d}^2}{\mathrm{d}\eta^2}g_2(\eta)\right)-e_2g_0(\eta)\left(\frac{\mathrm{d}}{\mathrm{d}\eta}f_1(\eta)\right)+2e_1f_2(\eta)\cdot\left(\frac{\mathrm{d}}{\mathrm{d}\eta}g_0(\eta)\right)+e_3\left(\frac{\mathrm{d}^2}{\mathrm{d}\eta^2}f_0(\eta)\right)+2e_1f_1(\eta)\cdot\left(\frac{\mathrm{d}}{\mathrm{d}\eta}g_1(\eta)\right)+2e_1f_0(\eta)\left(\frac{\mathrm{d}}{\mathrm{d}\eta}g_2(\eta)\right)+e_2\left(\frac{\mathrm{d}^2}{\mathrm{d}\eta^2}g_1(\eta)\right)-2e_1\left(g_2(\eta)\right)+\left(\frac{\mathrm{d}^2}{\mathrm{d}\eta^2}g_3(\eta)\right)+2e_2f_0(\eta)\left(\frac{\mathrm{d}}{\mathrm{d}\eta}g_1(\eta)\right)+e_2\left(\frac{\mathrm{d}^2}{\mathrm{d}\eta^2}f_1(\eta)\right)=0 \tag{27b}$$

$$f_3(-1)=0,\quad f_3(1)=0,\quad f_3'=0,\ f_3'(-1)=0 \tag{27c}$$

$$g_3(-1)=0,\quad g_3(1)=0 \tag{27d}$$

Solving Eqs. (24)−(27) with boundary conditions:

$$\begin{cases} f_0(\eta) = -\frac{1}{2}\eta^3 + \frac{3}{2}\eta \\ g_0(\eta) = 0 \end{cases} \tag{28}$$

$$\begin{cases} f_1(\eta) = d_1(\frac{1}{280}\eta^7 - \frac{3}{40}\eta^5 + \frac{39}{280}\eta^3 - \frac{19}{280}\eta) \\ g_1(\eta) = \frac{1}{2}e_1\eta^3 - \frac{1}{2}e_1\eta \end{cases} \tag{29}$$

$$f_2(\eta) = -\frac{3}{30800}{d_1}^2\eta^{11} + \frac{1}{420}{d_1}^2\eta^9 - \frac{1}{9800}(-35d_2 + 212{d_1}^2 - 35d_1)\eta^7 - \frac{1}{1400}(-139{d_1}^2 + 105d_2 + 105d_1 - 35e_1d_1)\eta^5 + \frac{1}{6}(-\frac{18461}{21560}{d_1}^2 + \frac{117}{140}d_2 + \frac{117}{140}d_1 - \frac{3}{10}e_1d_1)\eta^3 + (\frac{6767}{107800}{d_1}^2 - \frac{19}{280}d_2 - \frac{19}{280}d_1 + \frac{1}{40}e_1d_1)\eta \tag{30a}$$

$$g_2(\eta) = -\frac{1}{5880}(-105{e_1}^2 + 21e_1d_1)\eta^7 - \frac{1}{2800}(350{e_1}^2 - 210e_1d_1)\eta^5 - \frac{1}{840}(-420e_1 + 117e_1d_1 - 420e_2 + 455{e_1}^2)\eta^3 + (\frac{109}{168}{e_1}^2 + \frac{19}{280}e_1d_1 - \frac{1}{2}e_1 - \frac{1}{2}e_2)\eta \tag{30b}$$

The terms $f_3(\eta)$ and $g_3(\eta)$ are too long to be written in the above. So, the final expressions for $f(\eta)$ and $g(\eta)$ are

$$\begin{cases} f(\eta) = f_0(\eta) + f_1(\eta) + f_2(\eta) + f_3(\eta) \\ g(\eta) = g_0(\eta) + g_1(\eta) + g_2(\eta) + g_3(\eta) \end{cases} \tag{31}$$

Substituting $f(\eta)$ and $g(\eta)$ from Eq. (31) into Eqs. (10) and (11) yields the residuals $R_1(\eta, d_1, d_2, d_3)$ and $R_2(\eta, e_1, e_2, e_3)$. Then the functional $J_1$ and $J_2$ are obtained as the following:

$$\begin{cases} J_1(d_1, d_2, d_3) = \int_0^\infty R_1^2(\eta, d_1, d_2, d_3)\mathrm{d}\eta \\ J_2(e_1, e_2, e_3) = \int_0^\infty R_2^2(\eta, e_1, e_2, e_3)\mathrm{d}\eta \end{cases} \tag{32}$$

The constants $d_1$, $d_2$, $d_3$, $e_1$, $e_2$ and $e_3$ are obtained from Eq. (32) for the special case ($c_1$=$c_2$=$c_3$=$Re$=1):

$d_1$=0.03306062640,

$d_2$=−0.07733921182,

$d_3$=0.2353528166,

$e_1$=0.6879526470,

$e_2$=−0.01932908977,

$e_3$=1.500384566.

In order to validate the present solution of the problem and find the accuracy, the comparison between our solution and numerical result is done. An excellent agreement between the present OHAM and numerical solution is observed in Fig. 2, which confirms the validity of the proposed solution.

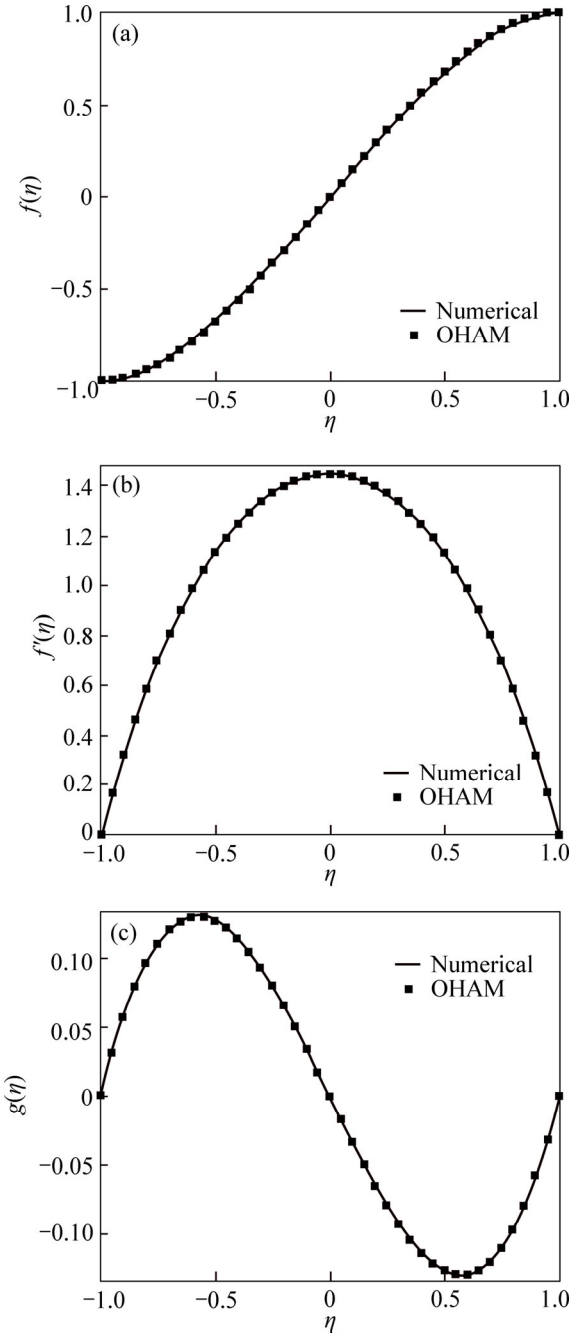


**Fig. 2** Comparison between OHAM solution and numerical results when $C_1$=$C_2$=$C_3$=$Re$=1: (a) $f(\eta)$; (b) $f'(\eta)$; (c) $g(\eta)$

## 5 Results and discussion

The graphical results are displayed to understand the effects of the Reynolds number, vortex viscosity, spin gradient viscosity and micro-interia density on the velocity profiles $f(\eta)$, $f'(\eta)$ and microrotation $g(\eta)$.

Figure 3 illustrates the behavior of streamwise and normal velocities and microrotation for different values of vortex viscosity parameter. Figure 3(a) shows that the values of normal velocity profile are positive in the first half region and negative in the second half region, which shows a reverse velocity near the boundaries of the two

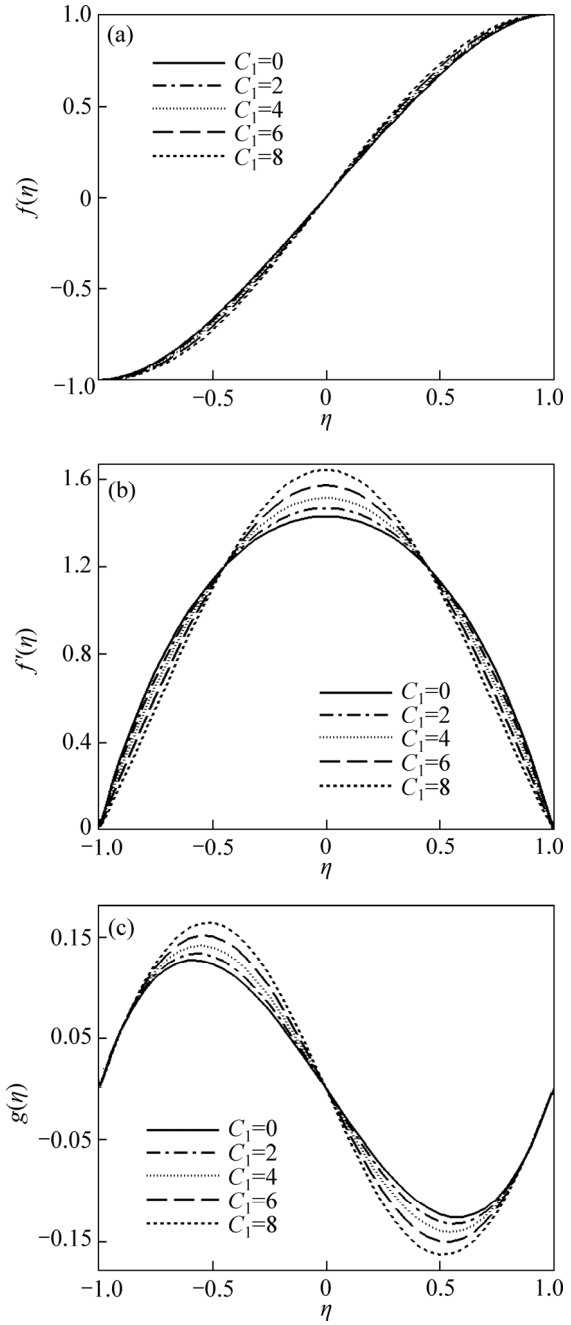


**Fig. 3** Normal velocity profile for different values of vortex viscosity ($C_1$) when $C_2$=$C_3$=$Re$=1: (a) $f(\eta)$; (b) $f'(\eta)$; (c) $g(\eta)$

disks. As a general trend, the normal velocity takes its dimensionless value 1 at the upper disk and −1 at the lower disk with a point of inflection on the central plane $z$=0, where the concavity is changed. The normal velocity profiles are concave downward in the lower half while they are concave upward in the upper half. Figure 3(b) depicts the behavior of streamwise velocity profile for different values of vortex viscosity. The streamwise velocity profiles are parabolic in nature for all the values of the vortex viscosity. The streamwise velocity increases near the central plane, while its profiles fall near the boundaries of the disks with an increase of $C_1$. The magnitude of the microrotation increases with the increase of vortex viscosity as seen in Fig. 3(c). The microrotation has opposite signs near the disks. The shear stresses at the two disks tend to rotate the fluid in opposite directions, and the point of zero microrotation marks the position across the disks where the effects of the opposite rotations balance each other.

Figure 4 illustrates the influence of spin-gradient viscosity on velocity and microrotation fields when $C_1$, $C_3$ and $Re$ are fixed at typical value of 1. As seen in Fig. 4(a), a slight increase near the upper disk and a slight decrease near the lower disk in $f$ are noted with an

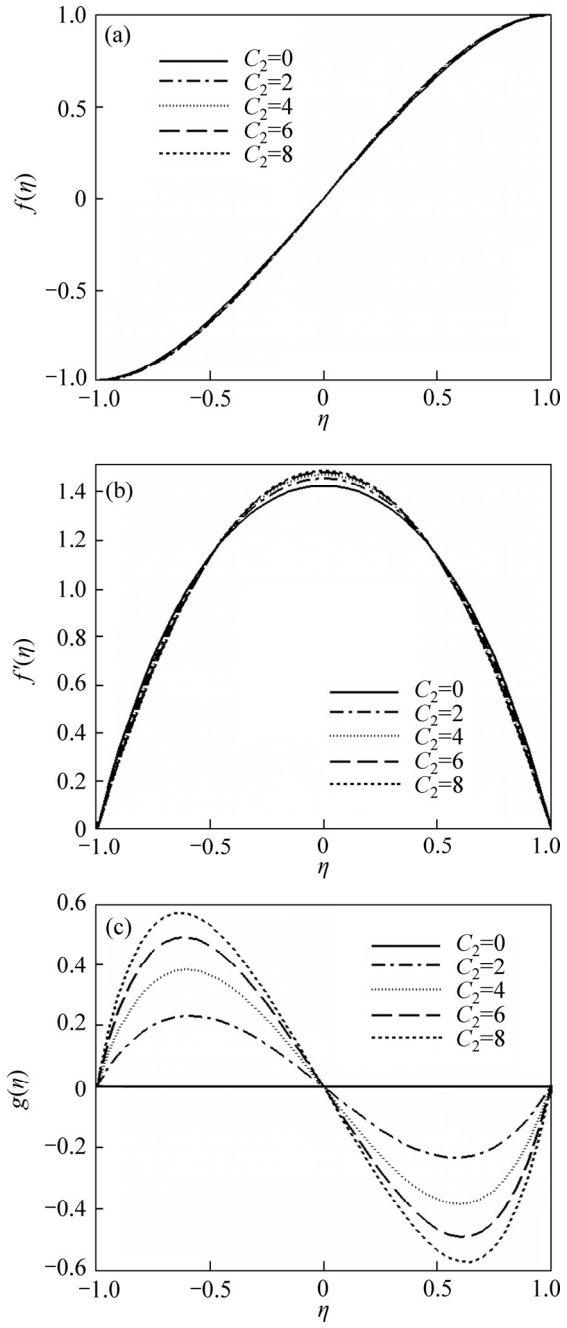


**Fig. 4** Normal velocity profile for different values of spin-gradient viscosity ($C_2$) when $C_1$=$C_3$=$Re$=1: (a) $f(\eta)$; (b) $f'(\eta)$; (c) $g(\eta)$

increase in the magnitude of spin-gradient viscosity. Figure 4(b) shows that by increasing $C_2$, the streamwise velocity decreases near the disks. The significant effect of spin-gradient viscosity on microrotation is seen in Fig. 4(c). An increase in the magnitude of the microrotation is observed with an increase in the values of the magnitude of spin-gradient viscosity.

From Fig. 5(a), it is clear that the normal velocity profile has no change for different values of micro-interia viscosity. Moreover, the axial velocity ($f'(\eta)$) does not have significant change by varying the values of $C_3$, as seen in Fig. 5(b). It is seen from Fig. 5(c) that the magnitude of the microrotation decreases with the increase in $C_3$.

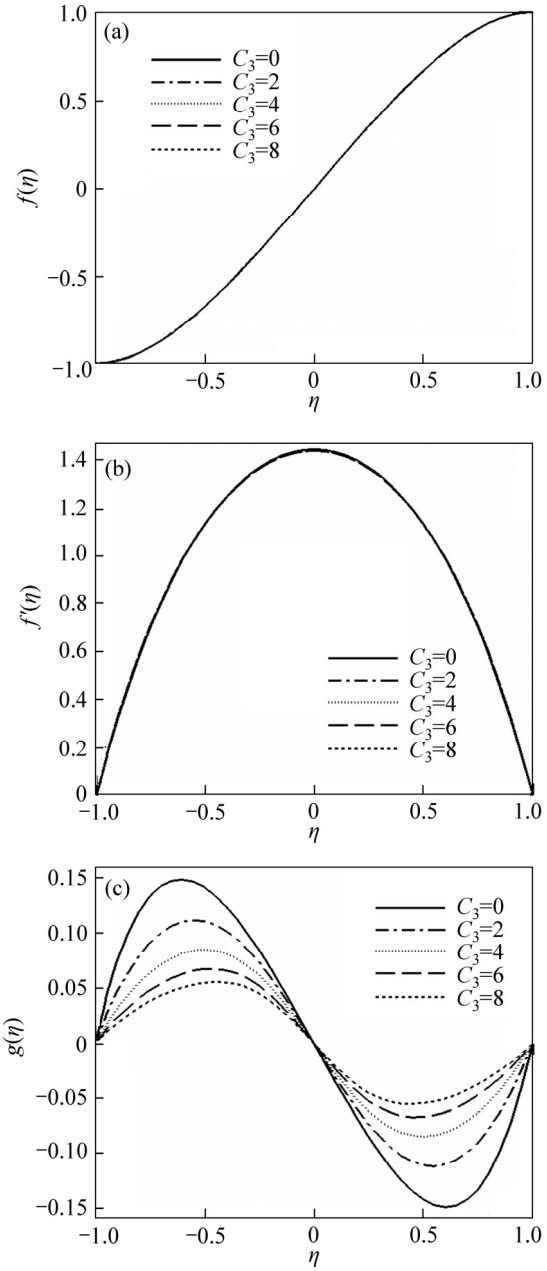


**Fig. 5** Normal velocity profile for different values of micro-inertia density ($C_3$) when $C_1$=$C_2$=$Re$=1: (a) $f(\eta)$; (b) $f'(\eta)$; (c) $g(\eta)$

The effect of Reynolds number on the flow velocities and the microrotation is investigated in Fig. 6. The results are obtained when $C_1$, $C_2$ and $C_3$ are fixed at 1. Figure 6(a) depicts the effects of Reynolds number on the normal velocity. The Reynolds number has an obvious effect on the normal velocity distribution for both suction and injection. For an increase in injections, the magnitude of normal velocity increases and a reverse phenomena may be noticed in the case of suction.

Figure 6(b) shows that the axial velocity is parabolic for the negative values of Reynolds number (injection), and for the cases $Re$>0, the axial velocity exhibits the characteristic flattering. Another point of Fig. 6(b) is that for the cases $Re$<0, as the imposed

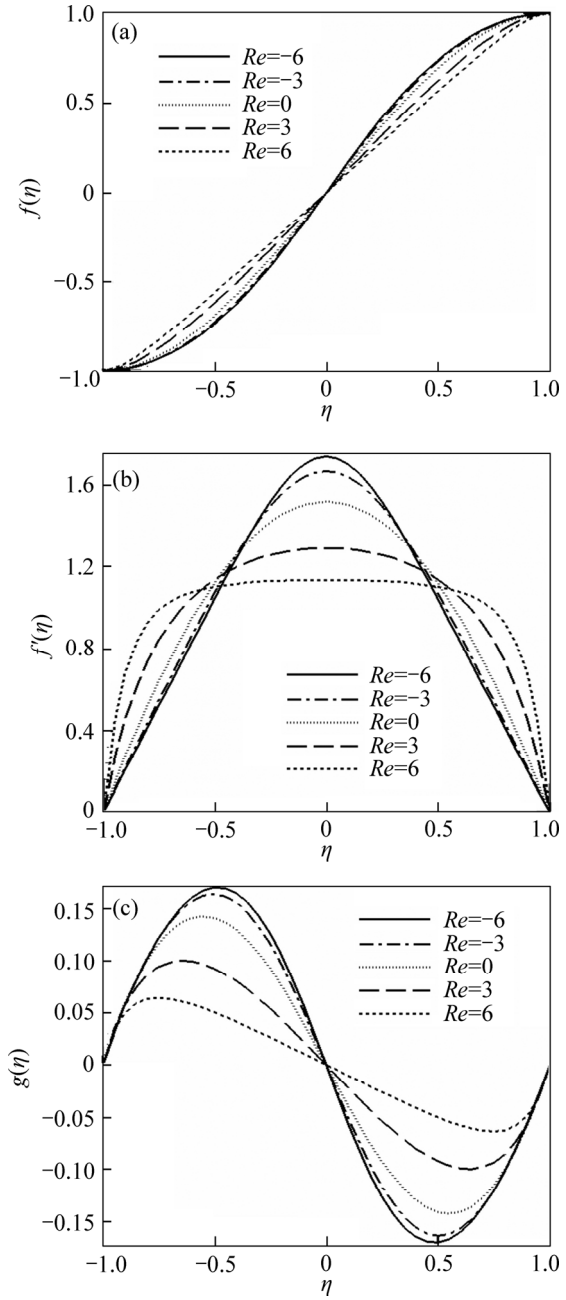


**Fig. 6** Normal velocity profile for different values of Reynolds Number ($Re$) when $C_1$=$C_2$=$C_3$=1: (a) $f(\eta)$; (b) $f'(\eta)$; (c) $g(\eta)$

injection through the disks increases, the fluid is pushed towards the central region between the disks, and therefore, the axial velocity increases significantly with the increase in *Re* in the magnitude. And for the cases *Re*>0, velocity decreases near the central plane and the fluid is pushed towards the boundaries by increasing *Re*. Figure 6(c) presents the influence of Reynolds number on the variation of the microrotation between two disks. For all cases, the point microrotation getting zero lies near the central plane and the extreme values are almost equal in magnitude. For the cases *Re*<0, an increase in the magnitude of the microrotation is observed with an increase in the values of the magnitude of Reynolds number and a reverse phenomenon is noticed in the case of *Re*>0 (suction).

## 6 Conclusions

1) Two dimensional micropolar flow between two porous disks is studied by optimal homotopy asymptotic method (OHAM). The approximate solutions for streamwise and normal velocities and microrotation are obtained by the proposed technique.

2) The present results are in excellent agreement with the numerical ones. Also this method is an efficient and accurate technique for finding science and engineering non-linear differential equations.

3) The streamwise velocity increases near the central plane by increasing the vortex viscosity parameter whereas its profiles fall near the boundaries of the disks.

4) Changing microrotation parameters does not have any significant effect on the axial velocity and they have slight effect on the normal velocity while they have significant effect on the microrotation profile $g(\eta)$.

5) The magnitude of the microrotation increases with the increase of injection velocity and a reverse phenomenon is noticed for the positive Reynolds number (suction).

## References


[1] KARMAN T V. Über laminare und turbulente reibung [J]. ZAMM-Journal of Applied Mathematics and Mechanics, 1921, 1: 233−252.

[2] ASHRAF M, ANWAR K M, SYED K S. Numerical investigations of asymmetric flow of a micropolar fluid between two porous disks [J]. Acta Mechanica Sinica, 2009, 25: 787−794.

[3] NAZIR A, MAHMOOD T. Analysis of flow and heat transfer of viscous fluid between contracting rotating disks [J]. Applied Mathematical Modelling, 2011, 35: 3154−3165.

[4] SI X H, ZHENG L C, ZHANG X X, SI X Y. Homotopy analysis method for the asymmetric laminar flow and heat transfer of viscous fluid between contracting rotating disks [J]. Applied Mathematical Modelling, 2012, 36: 1806−1820.

[5] IBRAHIM F. Unsteady flow between two rotating discs with heat transfer [J]. Journal of Physics D: Applied Physics, 1991, 24: 1293− 1299.

[6] ERSOY V H. An approximate solution for flow between two disks rotating about distinct axes at different speeds [J]. Mathematical Problems in Engineering, 2007, DOI: 10.1155/2007/ 36718.

[7] HATAMI M, SHEIKHOLESLAMI M, GANJI D D. Nanofluid flow and heat transfer in an asymmetric porous channel with expanding or contracting wall [J]. Journal of Molecular Liquids, 2014, 195: 230−239.

[8] HATAMI M, GANJI D D. Heat transfer and nanofluid flow in suction and blowing process between parallel disks in presence of variable magnetic field [J]. Journal of Molecular Liquids, 2014, 190: 159−168.

[9] ERINGEN A C. Theory of micropolar fluids [M]. DTIC Document, 1965: 22−48.

[10] ANWAR K M, ASHRAF M, SYED K S. Numerical solution of steady viscous flow of a micropolar fluid driven by injection between two porous disks [J]. Applied Mathematics and Computation, 2006, 179: 1−10.

[11] ASHRAF M, WEHGAL A. MHD flow and heat transfer of micropolar fluid between two porous disks [J]. Applied Mathematics and Mechanics, 2012, 33: 51−64.

[12] DARVISHI M T, KHANI F, AWAD F G, KHIDIR A A, SIBANDA P. Numerical investigation of the flow of a micropolar fluid through a porous channel with expanding or contracting walls [J]. Propulsion and Power Research, 2014, 3: 133−142.

[13] GHASEMI S E, JALILI PALANDI S, HATAMI M, GANJI D D. Efficient analytical approaches for motion of a spherical solid particle in plane couette fluid flow using nonlinear methods [J]. The Journal of Mathematics and Computer Science, 2012, 5(2): 97−104.

[14] GHASEMI S E, ZOLFAGHARIAN A, GANJI D D. Study on motion of rigid rod on a circular surface using MHPM [J]. Propulsion and Power Research, 2014, 3(3): 159−164.

[15] GHASEMI S E, HATAMI M, MEHDIZADEH A G R, GANJI D D. Electrohydrodynamic flow analysis in a circular cylindrical conduit using least square method [J]. Journal of Electrostatics, 2014, 72: 47−52.

[16] GHASEMI S E, HATAMI M , GANJI D D. Thermal analysis of convective fin with temperature-dependent thermal conductivity and heat generation [J]. Case Studies in Thermal Engineering, 2014, 4: 1−8.

[17] GHASEMI S E, VALIPOUR P, HATAMI M , GANJI D D. Heat transfer study on solid and porous convective fins with temperature-dependent heat generation using efficient analytical method [J]. Journal of Central South University, 2014, 21: 4592−4598.

[18] MARINCA V, HERISANU N. Application of optimal homotopy asymptotic method for solving nonlinear equations arising in heat transfer [J]. International Communications in Heat and Mass Transfer, 2008, 35: 710−715.

[19] MARINCA V, HERISANU N, BOTA C, MARINCA B. An optimal homotopy asymptotic method applied to the steady flow of a fourth-grade fluid past a porous plate [J]. Applied Mathematics Letters, 2009, 22: 245−251.

[20] GHASEMI S E, HATAMI M, GANJI D D. Analytical thermal analysis of air-heating solar collectors [J]. Journal of Mechanical Science and Technology, 2013, 27(11): 3525−3530.

[21] JONEIDI A, GANJI D D, BABAELAHI M. Micropolar flow in a porous channel with high mass transfer [J]. International Communications in Heat and Mass Transfer, 2009, 36: 1082−1088,.

[22] ESMAEILPOUR M, GANJI D D. Solution of the Jeffery–Hamel flow problem by optimal homotopy asymptotic method [J]. Computers & Mathematics with Applications, 2010, 59: 3405−3411.


**(Edited by FANG Jing-hua)**